PCCP

Accepted Manuscript

ROYAL SOCIETY OF CHEMISTRY

www.rsc.org/pccp

A new potential energy surface for the ground electronic state of LiH_2 system and dynamics studies on the $H(^2S) + LiH(X^1\Sigma^+) \rightarrow Li(^2S) + H_2(X^1\Sigma_g^+)$ reaction

Jiuchuang Yuan†, Di He†, Maodu Chen*

Key Laboratory of Materials Modification by Laser, Electron, and Ion Beams (Ministry of Education), School of Physics and Optoelectronic Technology, Dalian University of Technology, Dalian 116024, PR China

† These authors contributed equally to this work.

*Corresponding author. E-mail: mdchen@dlut.edu.cn (M.D. Chen)

Abstract

A new global potential energy surface (PES) is obtained for the ground electronic state of LiH_2 system based on high-level energies. The energy points are calculated at the multireference configuration interaction level with aug-cc-pVXZ (x=Q, 5) basis sets, and these energies are extrapolated to the complete basis set limit. The neural network method and hierarchical construction scheme are applied in the fitting process and the root mean square error of the fitting result is very small (0.004eV). The dissociation energies and equilibrium distances for $LiH(X^1\Sigma^+)$ and $H_2(X^1\Sigma_g^+)$ obtained from the new PES are in good agreement with the experimental data. On the new PES, the time-dependent wave packet studies for the $H(^2S)$ + $LiH(X^1\Sigma^+)$ → $Li(^2S)$ + $H_2(X^1\Sigma_g^+)$ reaction have been carried out. In this reaction, no threshold is found due to the absence of the energy barrier on the minimum energy path. The calculated integral cross sections are high at low collision energy and will decrease with the increase of the collision energy. The product molecule H_2 tends to be forward scattering due to direct reactive collisions, which becomes more evident at higher collision energies.

1 Introduction

In recent years, the lithium chemistry has received much attention due to its important position during the evolution of the primordial universe [1-9]. The formation and depletion of LiH molecular play an important part in galactic lithium production and stellar evolution [2, 3]. The H + LiH reaction is considered as an important pathway of the LiH depletion [4, 5]. Besides, the physical significance of the reactive system also make itself attractive. The LiH_2 system is the simplest form of the alkali metal-dihydrogen partners containing only five electrons which offers a good research object to nonadiabatic transition study. For these reasons, a flurry of studies have been carried out on LiH_2 chemical system during the past decade [10-29].

To study the reaction dynamics, it is necessary to construct the potential energy surface (PES) which describes the interaction of the molecular system. In the past decade, several three-dimensional ground-state ($^2A'$) PESs of LiH_2 system [10, 13, 17, 18, 26] have been constructed to investigate the dynamics of the reactive processes.

The first full three dimensional PES was developed by Dunne, Murrel, and Jemmer (DMJ) [10] using *ab initio* configuration interaction (CI) method and spectroscopic data. The energy data of approximately 300 randomly generated configurations of LiH_2 were sampled, and the augmented correlation consistent polarized valence double zeta basis (aug-cc-pVDZ) was employed in the calculation. The PES was fitted to a standard many-body form and the two-body parts were taken as extended Rydberg potentials. The root mean square error (RMSE) of the fitting result was 0.09 eV, and the maximum error was 0.36 eV. In 2003, Kim et al. [13] calculated energy data at the multireference configuration interaction (MRCI) level with complete active space self-consistent field (CASSCF) reference wave function. About 7000 points were selected, and interpolant moving least squares (IMLS)/Shepard scheme was used for interpolation of PES. With the increase of computing power, energy points with higher precision were calculated to construct the PES of this system. In 2009, Wernli et al. [17] reported a global three-dimensional

PES (Wernli PES), which was fitted by large scale calculated energy data (23300 points) in an analytic form (modified Aguado-Paniagua form). The energy data was calculated at MRCI level with CASSCF reference wave function, and correlation consistent polarized valence quadrupole zeta (cc-pVQZ) basis set was employed. In the same year, Prudente et al.[18] also structured an analytic PES (Prudente PES) to study the reaction dynamics of H + LiH reaction. The energy data was calculated using the full CI method with aug-cc-pVQZ basis set. Based on the energy data, the analytical PES function was obtained employing the many-body expansion, and the root means square deviation (rmsd) was 0.064 eV. In 2011, Hsiao et al. constructed PESs of 1A′ and 2A′ states for Li(2^2P) + H_2 reaction and carried out quasiclassical trajectory (QCT) calculations.[26] In the QCT calculation, the transition probability for the trajectories at the crossing seam region was assumed to be unity and trajectories changed to the lower surface for simplicity.

In recent years, Wernli PES [17] and Prudente PES [18] were widely applied to study the reaction dynamics. The small difference between the two PESs is the early-staged energy barrier on Prudente PES [18], which doesn't exist on Wernli PES [17]. Due to the difference, the physical pictures obtained from the two PESs were obviously different especially at low collision energy[29]. Therefore, for the title reaction, a more accurate PES is needed to obtain the reasonable dynamics results. In this work, we report an accurate global PES for the lowest doublet state of LiH_2 (^{2}A′) system. Normally, the quality of a PES is determined by the precision of the energy data and fitting method. For the high-precision energy data, we use expanded basis set in calculation. Up to now, many fitting methods have been developed, and the most common one is many-body expansion which is used widely to construct PESs [30-32]. In recent years, neural network (NN) method has received much attention as a powerful tool to construct PES for a wide range of systems [33, 34]. For example, in 2013, a high-precision PES for F+HD reaction was constructed using NN method, and the dynamics results calculated based on the PES were in very good agreement with experimental results.[35] In the end of this work, based on the new PES, the time-dependent wave packet (TDWP) calculation is carried out to study the dynamics

of the $H(^2S) + LiH(X^1\Sigma^+) \rightarrow Li(^2S) + H_2(X^1\Sigma_g^+)$ reaction.

2 Potential Energy Surface

2.1 *Ab initio* Calculations

The *ab initio* calculations have been carried out using the internally contracted MRCI [36, 37] with a CASSCF [38, 39] reference wavefunction. The CASSCF orbitals are obtained by employing the equally weighted state-averaged calculations for the ground state $1^2A'$ and the first excited state $2^2A'$ of LiH_2 system. Three valence electrons of LiH_2 molecule are included in eleven active orbitals (9a' + 2a''). Core-valence electron correlation is recovered including single excitations out of the doubly occupied Li($1s^2$) core orbitals. In both the CASSCF and MRCI calculations, the Dunning weighted correlation-consistent polarized core-valence quadruple-ζ and quintuple-ζ (cc-pwCVXZ, X=Q, 5) basis sets are employed for Li atom. At the same time, the augmented correlation consistent polarization valence quadruple and quintuple-ζ (aug-cc-pVXZ, X=Q, 5) basis sets are employed for H atom. The Jacobi coordinates are used for generating *ab initio* energy grid points. For the reaction H + LiH→Li + H_2, the reactant region is defined as $1.3 \le R_{LiH}/a_0 \le 20$, $0 \le R_{H\text{-}LiH}/a_0 \le 20$, $0 \le \theta$/degree ≤ 180, and the product region is chosen as $0.6 \le R_{HH}/a_0 \le 20$, $0 \le R_{Li\text{-}HH}/a_0 \le 20$, $0 \le \theta$/degree ≤ 90. All *ab initio* calculations in present work are performed with the MOLPRO package [40]. In this work, 12156 *ab initio* MRCI/(WCVQZ_{Li}/AVQZ_H) points are calculated to construct the PES, and 2234 [MRCI/(WCV5Z_{Li}/AV5Z_H) MRCI/(WCVQZ_{Li}/AVQZ_H)] *ab initio* points are calculated to extrapolate the correlation energy to the complete basis set (CBS) limit for improving the precision of this PES. The CBS limit correlation energy is extrapolated by using the formula [41]:

$$E_X^{corr} = E_\infty^{corr} + AX^{-3}, \qquad (1)$$

where the X=4 for the WCVQZ_{Li}/AVQZ_H basis and X=5 for the WCV5Z_{Li}/AV5Z_H basis. Then the CBS limit for the correlation energy is

$$E_\infty^{corr} = \left(E(\frac{MRCI}{WCV5Z_{Li}/AV5Z_H}) - E(\frac{MRCI}{WCVQZ_{Li}/AVQZ_H}) \right) \times \frac{4^{-3}}{4^{-3}-5^{-3}}, \qquad (2)$$

The Hartree-Fock (HF) energy is not extrapolated to the CBS because there is almost

no difference in the HF energy between $WCV5Z_{Li}/AV5Z_{H}$ and $WCVQZ_{Li}/AVQZ_{H}$ level for $LiH_2(1^2A')$. For the diatomic potential of H_2 and LiH, 54 and 92 points are calculated at MRCI/CBS level by using the method above mentioned, respectively

2.2 Fitting the potential energy surface

The total analytical expression of the global surface is presented as

$$V_{total}(\mathbf{R}) = \sum_{n} V_{n}^{(2)}(R_n) + V_{LiHH}^{(3)}(\mathbf{R}) \cdot f(\mathbf{R}), \quad (3)$$

where **R** is a collective variable of all internuclear distances. $V_n^{(2)}$ (n=HH, LiH_a, LiH_b) is the diatomic potential, and R_n is the bond distance of relevant diatomic. $V_{LiHH}^{(3)}$ is the three-body term. $f(\mathbf{R})$ is the switch function which is used in order to have a well-described PES in the asymptotic region, and it can be written as follows:

$$f(\mathbf{R}) = \prod_{n} \left(1 - \frac{1}{2} \left(1 + \tanh \left(\frac{R_n - R_d}{R_w} \right) \right) \right) \quad (4)$$

where n=HH, LiH_a, LiH_b. R_d is the position to switch and R_w is the switch strength constant.

The NN method[42] is used to build both of the two–body potential energy and the three-body term. The idea of NN is inspired by central nervous system of animal. In an NN, the basic unit is a neuron which receives input signals and emits an output signal as a synapse. For a neuron, the output signal y can be written as

$$y = \phi \left(\sum_{i=1}^{N} w_i x_i + b \right), \quad (5)$$

where x_i (i=1, …, N) is the input signals, w_i is the connection weight, b is a bias, and ϕ is a transfer function. To date, there are many NN types developed for various purposes, and the most common one is the feed-forward NN which is used to fit two-body and three-body terms in this PES. In order to take account of computational efficiency and fitting precision, a series of tests have been taken to determine the structures of NNs.

The two-body potential energies ($V_{HH}^{(2)}$ and $V_{LiH}^{(2)}$) are fitted based on the energy points obtained at MRCI/CBS level. For two-body potential energies, the NNs include two hidden layers and there are five neurons in each hidden layer. The precision of the fitting is very high and the RMSEs are extremely small (1.0×10^{-7} eV for $V_{HH}^{(2)}$ and 3.6×10^{-7} eV for $V_{LiH}^{(2)}$).

For the PES, the three-body term is critical factor which determines the quality of the PES. In order to improve the precision and save the consumption of computation, the hierarchical construction (HC) scheme[43] is used to construct the three-body term $V_{LiHH}^{(3)}(\mathbf{R})$. In the HC method, a high accuracy PES can be structured by summing a low accuracy PES and a different PES for high and low accuracy *ab initio* methods. The low accuracy PES is fitted based on dense *ab initio* points, and the different PES is fitted based on sparse *ab initio* points. In this work, the three-body term $V_{LiHH}^{(3)}(\mathbf{R})$ at MRCI/CBS level can be expressed as

$$V_{LiHH}^{(3)}(\mathbf{R}) = V_{QZ}^{(3)}(\mathbf{R}) + \Delta V_{CBS\text{-}QZ}^{(3)}(\mathbf{R}), \quad (6)$$

where $V_{QZ}^{(3)}(\mathbf{R})$ is fitted based on 12156 *ab initio* MRCI/(WCVQZ$_{Li}$/AVQZ$_{H}$) three-body points, and $\Delta V_{CBS\text{-}QZ}^{(3)}(\mathbf{R})$ is fitted based on 2234 difference values between three-body potential energies at MRCI/CBS and MRCI/(WCVQZ$_{Li}$/AVQZ$_{H}$) levels. $V_{QZ}^{(3)}(\mathbf{R})$ and $\Delta V_{CBS\text{-}QZ}^{(3)}(\mathbf{R})$ are fitted by NN method respectively, and two hidden layers (11 neurons in first hidden layer, 12 neurons in second hidden layer) are included in the NNs. For solving the problem of adaptation of permutation symmetry in three-body potential energies, low-order permutation invariant polynomials (PIPs)[44, 45] are used as inputs for NNs.

By summing the two-body potential energies and three-body term as formula (3), a high-accuracy PES V_{total} is obtained with the RMSE only 0.004 eV.

2.3 Features of LiH_2 Potential Energy Surface

Table 1 shows the spectroscopic constants of $LiH(X^1\Sigma^+)$ and $H_2(X^1\Sigma_g^+)$ obtained from the new PES, as compared with the experimental data[46, 47]. The theoretical results obtained from the other two PESs [17, 18] are also listed in the table. It can be found that our results agree very well with the experimental data, which indicates that the new PES gives a good description of the two-body potential energy. The fitted bond lengths of LiH and H_2 are almost the same as experiment data. The bond energies are slightly higher than the experimental results (25.2 cm^{-1} for H_2 and 7.6 cm^{-1} for LiH). The calculated frequency and anharmonicity constant are close to the experiment data. Figure 1 shows the topographical features of three-dimensional ground PES at four different Li–H–H angles (180 °, 135 °, 90 °, and 45 °). The PESs are smooth over the whole configuration space. There are two valleys in each of the four surfaces: the left valley and right valley correspond to product of Li+ H_2 and reactant of H + LiH respectively. The left one is deeper than the right one because the reaction of H + LiH → Li + H_2 is exothermic. Figure 2 shows the minimum energy paths (MEPs) from LiH to H_2 at four different approaching angles. It clearly shows that there is no obvious barrier or well along the pathway, which is similar as the PES obtained by Wernli et al[17]. It implies that no threshold exists in the reaction of $H(^2S)$ + $LiH(X^1\Sigma^+)$ → $Li(^2S)$ + $H_2(X^1\Sigma_g^+)$. The exothermicity for the title reaction is 2.235 eV. The zero point energy of reactant LiH is 0.086 eV, and the zero point energy of product H_2 is 0.272 eV. So the exothermicity is 2.049 eV when the zero point energy is taken into account. Figure 3(a) shows a color plot of potential energy for a Li atom moving around a H_2 diatom with bond length fixed at the equilibrium distance (0.7414 angstrom), which lies along the x-axis with the center of the bond fixed at the origin. In the plot, the energy is set as zero when the atom is far away from the diatom. As seen in the figure, there is no well or barrier, and the Li atom is always repulsed by the H_2 molecule wherever the Li atom is. Similarly, Figure 3(b) shows the plot of potential energy when H atom moving around the LiH diatom with bond distance fixed at its equilibrium geometry (1.5957 angstrom). There exists a deep well around

the fixed H atom. When the H atom gets into the region of the well with low collision energy, it tends to be attracted by the fixed H atom. We conclude that the well plays an important role in the reaction of $H(^2S) + LiH(X^1\Sigma^+) \rightarrow Li(^2S) + H_2(X^1\Sigma_g^+)$, particularly at low collision energy.

3 Dynamical Calculations

On this new PES, the dynamics of $H(^2S) + LiH(X^1\Sigma^+) \rightarrow Li(^2S) + H_2(X^1\Sigma_g^+)$ reaction is investigated using the TDWP method which has been applied widely in many reactive systems[30, 48-52]. Detailed discussions on TDWP method can be found in relevant literatures [49, 53], and here we give a brief introduction. The reactant Jacobi coordinates is applied in the body fixed representation and the Hamiltonian can be written as

$$\hat{H} = -\frac{\hbar^2}{2\mu_R}\frac{\partial^2}{\partial R^2} - \frac{\hbar^2}{2\mu_r}\frac{\partial^2}{\partial r^2} + \frac{(\hat{J}-\hat{j})^2}{2\mu_R R^2} + \frac{\hat{j}^2}{2\mu_r r^2} + \hat{V} \quad , \qquad (7)$$

where R is the distance from H atom to the mass center of LiH molecule, and r is the bond length of LiH molecule. μ_R and μ_r are the corresponding reduced masses associated with R and r coordinates. $\hat{J}$ and $\hat{j}$ are the angular momentum operators of LiH_2 system and reactant diatom molecule. $\hat{V}$ represents the potential energy of LiH_2 system. The state-to-state S-matrix $S^{J\epsilon}_{vjK\leftarrow v_0 j_0 K_0}(E)$ is extracted using the reactant coordinate based method[54]. The state-to-state reaction probability is calculated by

$$P^J_{vj\leftarrow v_0 j_0} = \frac{1}{2j_0+1}\sum_{K,K_0}\left|S^J_{vjK\leftarrow v_0 j_0 K_0}\right|^2 . \qquad (8)$$

The state-to-state integral cross sections (ICSs) and differential cross sections (DCSs) are obtained by

$$\sigma_{vj\leftarrow v_0 j_0} = \frac{\pi}{(2j_0+1)k^2_{v_0 j_0}}\sum_K\sum_{K_0}\sum_J(2J+1)\left|S^J_{vjK\leftarrow v_0 j_0 K_0}\right|^2 \qquad (9)$$

and

$$\frac{d\sigma_{vj\leftarrow v_0 j_0}(\theta,E)}{d\Omega}=\frac{1}{(2j_0+1)}\sum_K\sum_{K_0}\left|\frac{1}{2ik_{v_0 j_0}}\sum_J(2J+1)d^J_{KK_0}(\theta)S^J_{vjK\leftarrow v_0 j_0 K_0}\right|^2, \quad (10)$$

where θ is the scattering angle. The rovibrational state of the reactant molecule LiH is set as $v_0 = 0$, $j_0 = 0$. In the TDWP method, the parameters those are determined through numerous tests are listed in the Table 2.

Figure 4 shows the total reaction probabilities of $H(^2S) + LiH(X^1\Sigma^+) \rightarrow Li(^2S) + H_2(X^1\Sigma_g^+)$ reaction with different total angular momentum quantum numbers as a function of collision energy. For the case of total angular momentum quantum number J = 0, there is no threshold in the reaction probability. It implies the reaction is spontaneous. As J value increases, the threshold appears due to the emergence of centrifugal barrier. There exist a mass of the resonance structures on the curves of reaction probability, which is an important signal of quantum effect. Similar features have also been reported in previous works [18, 27, 28]. Padmanaban et al. have studied [19, 21] resonance structures, and they found the resonance structures correspond to the metastable vibrational levels of LiH_2 system[21]. As the collision energy increases, the resonance structures get less pronounced because the reactive collisions become more direct. For comparison purposes, the reaction probabilities obtained on Prudente PES [18] and Wernli PES [17] using TDWP method are also shown in Figure 4. The applied numerical parameters are as same as those in the TDWP calculations on the present PES. The reaction probabilities calculated on Prudente PES [18] are significantly different from the other two results, because on the PES there exists an early-staged energy barrier [29]. The similar early-staged energy barrier has not been found on the present PES and Wernli PES [17]. The results obtained on present PES and Wernli PES [17] are similar at most of the collision energy but show significant difference at very low collision energy. It can be explained by the fact that the calculated result of reaction dynamics is sensitive to PES at low collision energy. The reaction probabilities obtained on present PES are higher at very low collision energy, thus the system is easier to react at a low temperature region.

In the TDWP calculation, the maximal total angular momentum quantum numbers is J=53, and its threshold is slightly higher than 0.5 eV which is the upper collision energy limit in the calculation of ICS. The total ICS of $H(^2S) + LiH(X^1\Sigma^+) \rightarrow Li(^2S) + H_2(X^1\Sigma_g^+)$ reaction as a function of collision energy is shown in Figure 5. As shown in the figure, no threshold exists due to the absence of an energy barrier on the minimum energy path. At low collision energy, the ICS value is high and decreases with the increasing collision energy. It can be explained by the feature of the PES. At low collision energy, the H atom moves to the LiH molecule slowly, and H atom will be attracted to another H atom when it gets into the region of the well mentioned in Figure 3(b). The LiH_2 system has enough time to adjust to produce the H_2 molecule. However, as the collision energy increases, the time of adjustment gets shorter, which leads to the decrease of ICS. At low collision energy, several peaks can be found on the ICS resulting from the resonance effect. To get the information of vibrational states of product H_2 molecule, the ICSs of the first four vibrational states ($v' = 0$ to 3) are also presented in the figure. The ICS values of $v'= 1$ and 2 are larger than those of $v' = 0$ and 3, because the exothermicity is large enough to vibrationally excite product H_2 molecule.

Figure 6 shows the total ICS compared with the results obtained on Wernli PES [17] and Prudente PES [18] using TDWP method. The ICS obtained on Prudente PES [18] is lower than the other two results which can attribute to the early-staged energy barrier. At high collision energy, all the ICSs decrease with collision energy increasing and our result is almost the same as that obtained on Wernli PES [17]. At low collision energy, compared with the ICS obtained on Wernli PES [17], our result is significantly higher and resonance peaks are more obvious. This again illustrates the importance of PES accuracy to reaction dynamics at low collision energy, because a small difference in the PES might lead to a significant difference in reaction dynamics.

To study the angular distribution of the product, DCSs at three collision energies (0.1 eV, 0.3 eV and 0.5 eV) are calculated and shown in Figure 7. The DCS results indicate that the product molecule tends to forward scattering. For the $H(^2S)$ +

$LiH(X^1\Sigma^+) \rightarrow Li(^2S) + H_2(X^1\Sigma_g^+)$ reaction, no potential well exists on the minimum energy path, so most reactive collisions are direct collisions. Therefore, the system doesn't have enough time to wash away the initial memory of the reactant. It leads to an obvious bias in the angular distribution of the product H_2 molecule. With the collision energy increasing, the trend of forward scattering gets more apparent because the reactive collisions get more direct.

4 Conclusion

In this work, we reported a new PES of ground electronic state of LiH_2 system based on high-level energies. The *ab initio* energies are calculated at the MRCI level with aug-cc-pVXZ (X=Q, 5) basis sets and the energies at CBS limit are obtained using these *ab initio* energies. The NN method is used to structure both of the two–body potential energy and the three-body term, and the HC scheme is used to construct the three-body term. The RMSE of the fitting result is only 0.004 eV. The spectroscopic constants for $LiH(X^1\Sigma^+)$ and $H_2(X^1\Sigma_g^+)$ obtained from the new PES agree very well with the experimental data. The calculation of TDWP is carried out for the $H(^2S) + LiH(X^1\Sigma^+) \rightarrow Li(^2S) + H_2(X^1\Sigma_g^+)$ reaction on the new PES. The reaction probabilities, ICSs and DCSs of the title reaction are calculated. The curves of reaction probability show a mass of resonance structures corresponding to the metastable vibrational levels of LiH_2 system. The resonance structures get less prominent with the collision energy increasing, because the reaction prefers direct collisions. No threshold exists in the reaction due to the absence of the energy barrier on the minimum energy path. At low collision energy, the ICS value is high and decreases with collision energy increasing. At low collision energy, there are several peaks on the total ICS curve, which is a typical characteristic of the resonance. The ICS values of $v' = 1$ and 2 are larger than those of $v' = 0$ and 3, because the exothermicity is large enough to vibrationally excite the product H_2 molecule. The DCS results indicate that the product molecule tends to be forward scattering due to the direct reactive collisions. With the collision energy increasing, the tendency of

forward scattering gets more pronounced because the reactive collisions are more direct.

Acknowledgments

This work was supported by the National Natural Science Foundation of China (Grant No. 11374045), the Fundamental Research Funds for the Central Universities (Grant No. DUT13ZD207), and Program for New Century Excellent Talents in University (Grant No. NCET-12-0077).

Table 1 The spectroscopic constants for $LiH(X^1\Sigma^+)$ and $H_2(X^1\Sigma_g^+)$ obtained from the new PES compared with the experimental data[46, 47] and results obtained on Wernli PES and Prudente PES [17, 18].

		Experimental	This work	Prudente PES	Wernli PES
$H_2(X^1\Sigma^+_g)$	R_e (Å)	0.7414	0.7414	0.7416	0.7420
	D_e (cm^{-1})	38288.0	38313.2	38181.5	38521.0
	ω_e (cm^{-1})	4401.21	4411.77	--	4463.55
	$\omega_e x_e$ (cm^{-1})	121.33	124.44	--	124.87
$LiH(X^1\Sigma^+)$	R_e(Å)	1.5956	1.5957	1.6075	1.6081
	D_e (cm^{-1})	20288.7	20296.3	20092.3	19968.0
	ω_e (cm^{-1})	1405.65	1402.56	--	1297.58
	$\omega_e x_e$ (cm^{-1})	23.20	23.05	--	21.71

Table 2. Numerical parameters used in the TDWP calculations. (Atomic units are used)

$H(^2S) + LiH(X^1\Sigma^+) \rightarrow Li(^2S) + H_2(X^1\Sigma_g^+)$	
Grid/basis range and size	$R \in [0.01, 25.0]$, N_R=199 $r \in [0.01, 20.0]$, N_r=149 N_j=199
Initial wave packet $\exp\left[-\frac{(R-R_c)^2}{2\Delta_R^2}\right]\cos(k_0 R)$	R_c=16.5 Δ_R=0.25 $k_0 = \sqrt{2E_0\mu_R}$ with E_0=0.5 eV
Total propagation time	30000 iterations
Highest J value	53

[1] D. Galli, and F. Palla, Astron. Astrophys. **335**, 403 (1998).
[2] M. Signore, G. Vedrenne, P. Debernardis, V. Dubrovich, P. Encrenaz, R. Maoli, S. Masi, G. Mastrantonio, B. Melchiorri, F. Melchiorri, and P. E. Tanzilli, Astrophys. J. Suppl. Ser. **92**, 535 (1994).
[3] R. Maoli, F. Melchiorri, and D. Tosti, Astrophys. J. **425**, 372 (1994).
[4] P. C. Stancil, and A. Dalgarno, Astrophys. J. **479**, 543 (1997).
[5] P. C. Stancil, S. Lepp, and A. Dalgarno, Astrophys. J. **458**, 401 (1996).
[6] V. K. Dubrovich, and A. A. Lipovka, Astron. Astrophys. **296**, 301 (1995).
[7] S. Lepp, and J. M. Shull, Astrophys. J. **280**, 465 (1984).
[8] S. Lepp, P. C. Stancil, and A. Dalgarno, J. Phys. B-At. Mol. Opt. Phys. **35**, R57 (2002).
[9] E. Bodo, F. A. Gianturco, and R. Martinazzo, Phys. Rep. **384**, 85 (2003).
[10] L. J. Dunne, J. N. Murrell, and P. Jemmer, Chem. Phys. Lett. **336**, 1 (2001).
[11] N. J. Clarke, M. Sironi, M. Raimondi, S. Kumar, F. A. Gianturco, E. Buonomo, and D. L. Cooper, Chem. Phys. **233**, 9 (1998).
[12] H. S. Lee, Y. S. Lee, and G. H. Jeung, J. Phys. Chem. A **103**, 11080 (1999).
[13] K. H. Kim, Y. S. Lee, T. Ishida, and G. H. Jeung, J. Chem. Phys. **119**, 4689 (2003).
[14] H. Berriche, J. Mol. Struc-Theochem **682**, 89 (2004).
[15] H. Berriche, and C. Tlili, J. Mol. Struc-Theochem **678**, 11 (2004).
[16] E. Bodo, F. A. Gianturco, R. Martinazzo, and M. Raimondi, Eur. Phys. J. D **15**, 321 (2001).
[17] M. Wernli, D. Caruso, E. Bodo, and F. A. Gianturco, J. Phys. Chem. A **113**, 1121 (2009).
[18] F. V. Prudente, J. M. C. Marques, and A. M. Maniero, Chem. Phys. Lett. **474**, 18 (2009).
[19] R. Padmanaban, and S. Mahapatra, J. Theor. Comput. Chem. **5**, 871 (2006).
[20] R. Padmanaban, and S. Mahapatra, J. Phys. Chem. A **110**, 6039 (2006).
[21] R. Padmanaban, and S. Mahapatra, J. Chem. Phys. **117**, 6469 (2002).
[22] P. Defazio, C. Petrongolo, P. Gamallo, and M. Gonzalez, J. Chem. Phys. **122**, 214303 (2005).
[23] K. C. Lin, and R. Vetter, Int. Rev. Phys. Chem. **21**, 357 (2002).
[24] T. Roy, T. R. Rao, and S. Mahapatra, Chem. Phys. Lett. **501**, 174313 (2011).
[25] S. Gomez-Carrasco, L. Gonzalez-Sanchez, N. Bulut, O. Roncero, L. Banares, and J. F. Castillo, Astrophys. J. **784**, 55 (2014).
[26] M. Hsiao, K. Lin, and Y. Hung, J. Chem. Phys. **134**, 034119 (2011).
[27] T. Roy, and S. Mahapatra, J. Chem. Phys. **136**, 174313 (2012).
[28] R. Padmanaban, and S. Mahapatra, J. Chem. Phys. **121**, 7681 (2004).
[29] G. Sha, J. Yuan, C. Meng, and M. Chen, Chem. Res. Chin. Univ. **29**, 956 (2013).
[30] Y. Li, J. Yuan, M. Chen, F. Ma, and M. Sun, J. Comput. Chem. **34**, 1686 (2013).
[31] Y. Q. Li, F. C. Ma, and M. T. Sun, J. Chem. Phys. **139**, 154305 (2013).
[32] Y. Q. Li, Y. Z. Song, P. Song, Y. Z. Li, Y. Ding, M. T. Sun, and F. C. Ma, J. Chem. Phys. **136**, 194705 (2012).
[33] C. M. Handley, and P. L. A. Popelier, J. Phys. Chem. A **114**, 3371 (2010).
[34] J. Behler, Phys. Chem. Chem. Phys. **13**, 17930 (2011).
[35] T. Wang, J. Chen, T. Yang, C. Xiao, Z. Sun, L. Huang, D. Dai, X. Yang, and D. H. Zhang, Science **342**, 1499 (2013).
[36] H. J. Werner, and P. J. Knowles, J. Chem. Phys. **89**, 5803 (1988).
[37] P. J. Knowles, and H.J. Werner, Chem. Phys. Lett. **145**, 514 (1988).
[38] H. J. Werner, and P. J. Knowles, J. Chem. Phys. **82**, 5053 (1985).

[39] P. J. Knowles, and H. J. Werner, Chem. Phys. Lett. **115**, 259 (1985).
[40] MOLPRO: http://www.molpro.net/.
[41] D. G. Truhlar, Chem. Phys. Lett. **294**, 45 (1998).
[42] H. Rabitz, and O. F. Alis, J. Math. Chem. **25**, 197 (1999).
[43] B. Fu, X. Xu, and D. H. Zhang, J. Chem. Phys. **129**, 011103 (2008).
[44] B. Jiang, and H. Guo, J. Chem. Phys. **139**, 054112 (2013).
[45] B. J. Braams, and J. M. Bowman, Int. Rev. Phys. Chem. **28**, 577 (2009).
[46] K. P. Huber, and G. Herzberg, *Constants of diatomic molecules* (Springer, 1979).
[47] W. C. Stwalley, and W. T. Zemke, J. Phys. Chem. Ref. Data **22**, 87 (1993).
[48] Z. Sun, L. Liu, S. Y. Lin, R. Schinke, H. Guo, and D. H. Zhang, Proc. Natl. Acad. Sci. **107**, 555 (2010).
[49] Z. Sun, S. Y. Lee, H. Guo, and D. H. Zhang, J. Chem. Phys. **130**, 174102 (2009).
[50] Z. Sun, W. Yang, and D. H. Zhang, Phys. Chem. Chem. Phys. **14**, 1827 (2012).
[51] D. Cheng, J. Yuan, and M. Chen, J. Phys. Chem. A **118**, 55 (2013).
[52] J. Yuan, D. Cheng, and M. Chen, RSC. Adv. **4**, 36189 (2014).
[53] Z. Sun, H. Guo, and D. H. Zhang, J. Chem. Phys. **132**, 084112 (2010).
[54] Z. Sun, X. Lin, S. Y. Lee, and D. H. Zhang, J. Phys. Chem. A **113**, 4145 (2009).

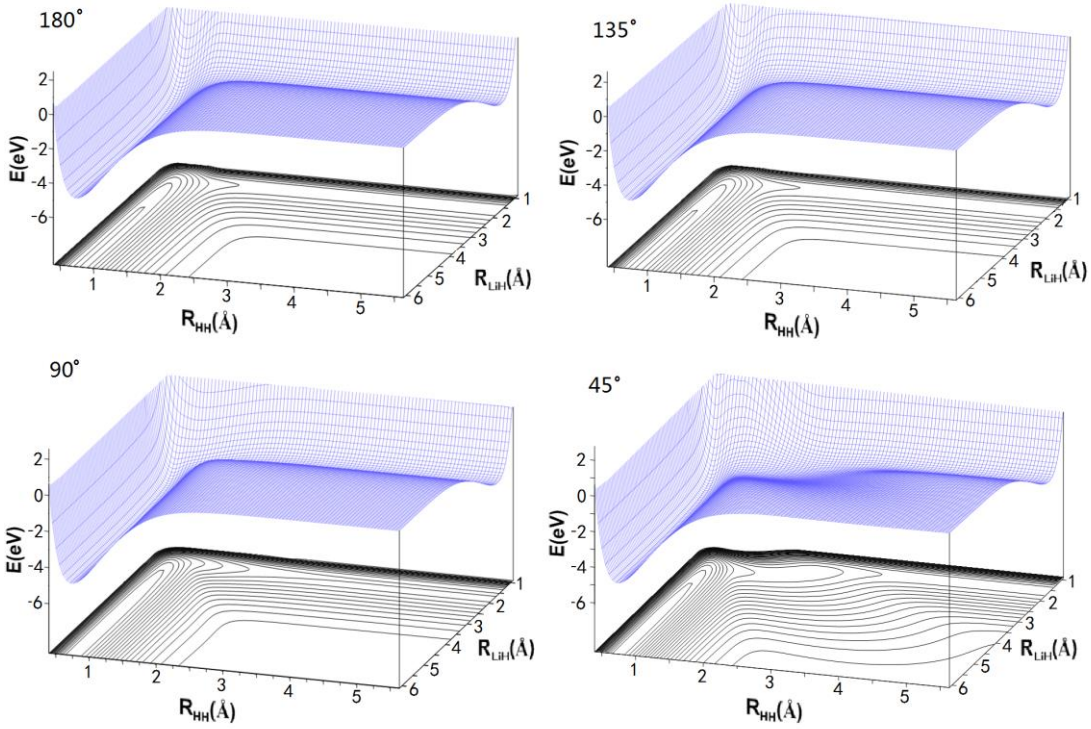

Fig. 1 Potential energy surfaces for the four Li-H-H angles 180°, 135°, 90° and 45°.

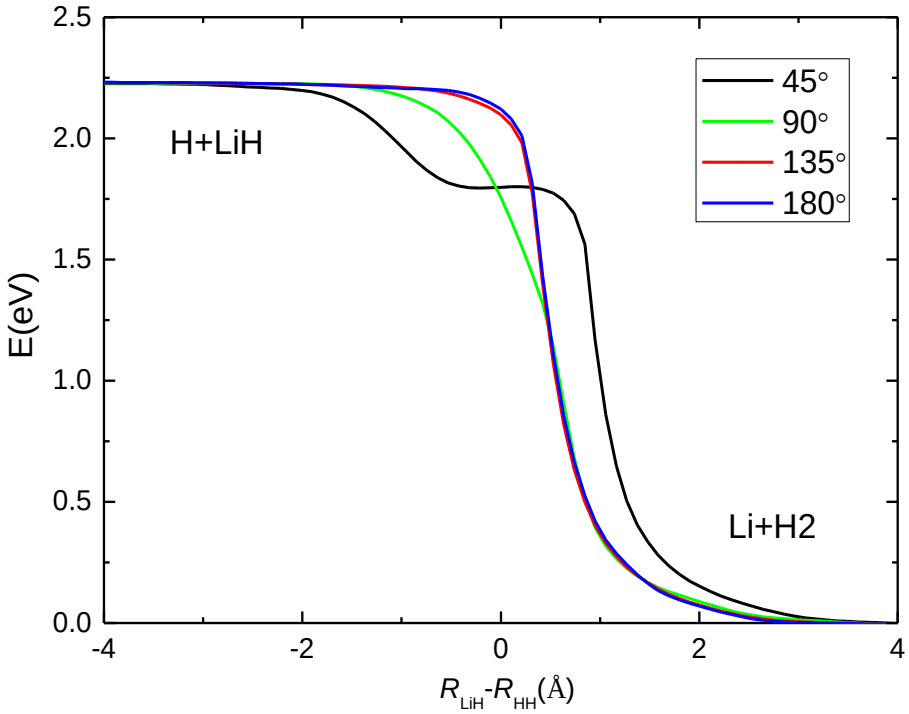

Fig. 2 Minimum energy paths for the new PES at four Li-H-H angles.

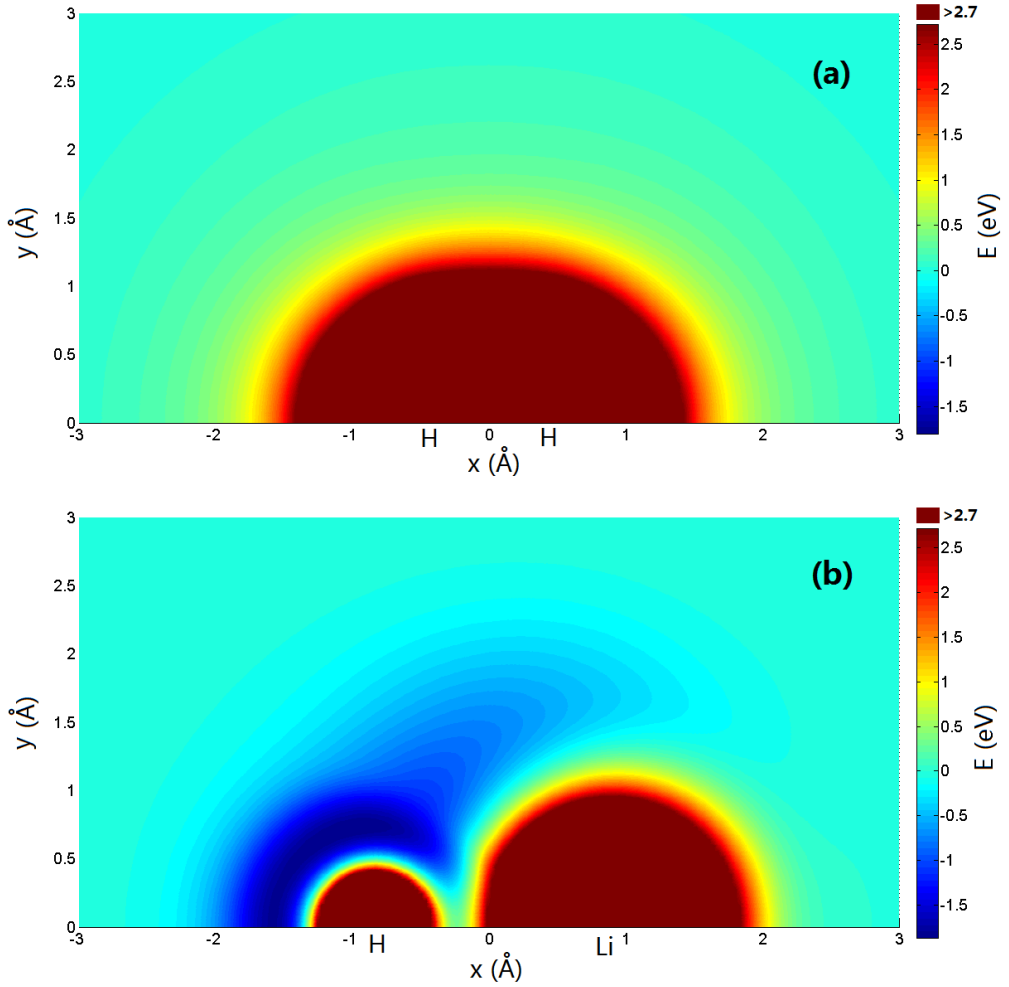

Fig. 3 (a) Color plot of the energy when the Li atom moving around H_2 diatom with bond length fixed at R_{HH} = 0.7414 angstrom (this lies along the x-axis with the center of the bond fixed at the origin). (b) Color plot of the energy when the H atom moving around HLi diatom with bond length fixed at R_{HLi} = 1.5957 angstrom.

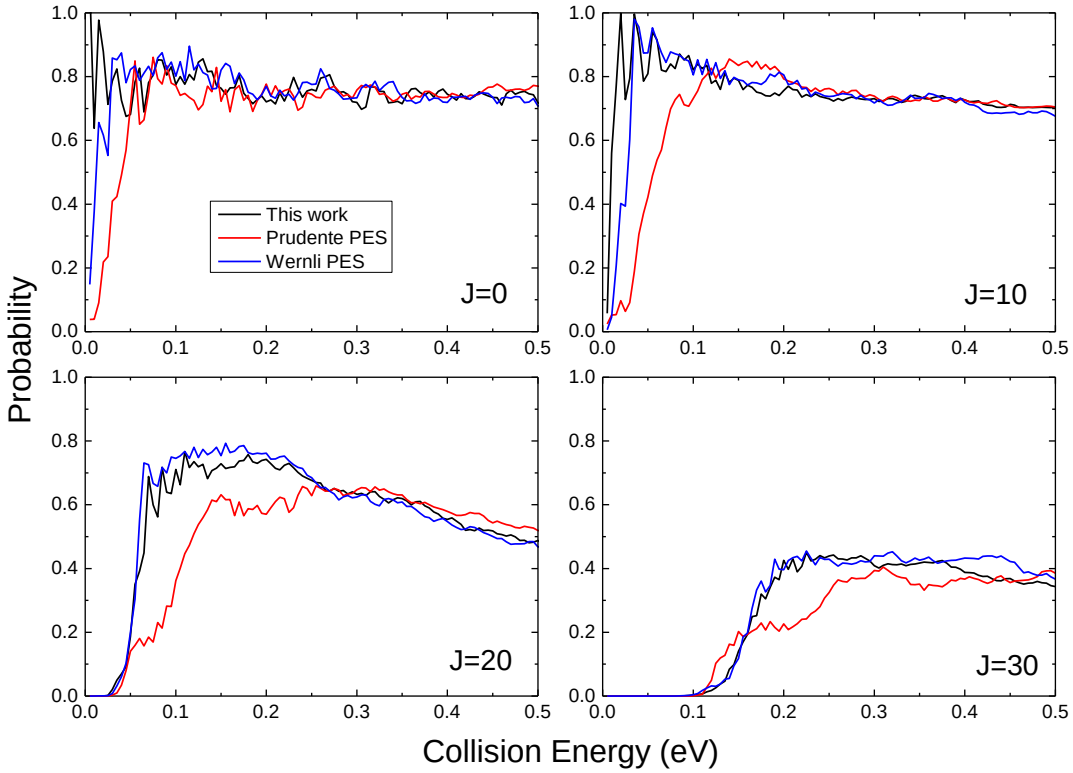

Fig. 4 Total reaction probabilities of the $H(^2S) + LiH(X^1\Sigma^+) \rightarrow Li(^2S) + H_2(X^1\Sigma_g^+)$ reaction calculated by the TDWP method using the present PES, Prudente PES [Ref. 18] and Wernli PES [Ref. 17].

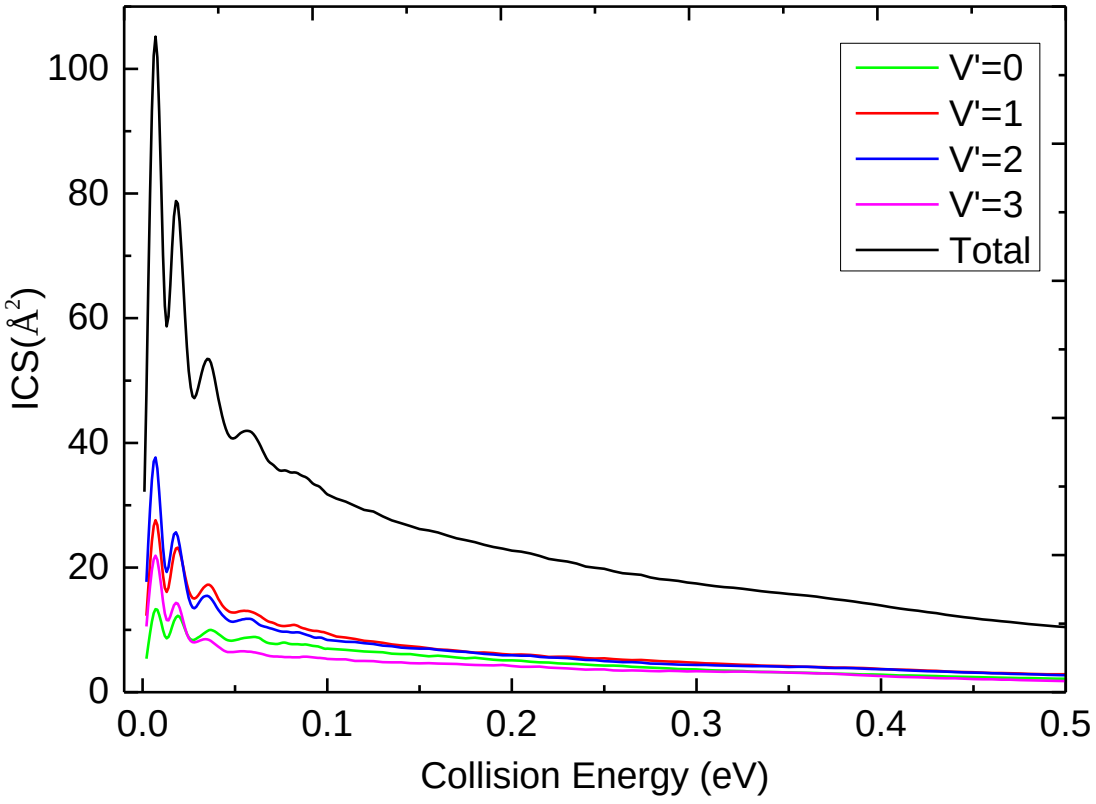

Fig. 5 Total and vibrationally resolved ICSs of the H(^{2}S) + LiH($X^1\Sigma^+$) → Li(^{2}S) + $H_2(X^1\Sigma_g^+)$ reaction calculated by TDWP method.

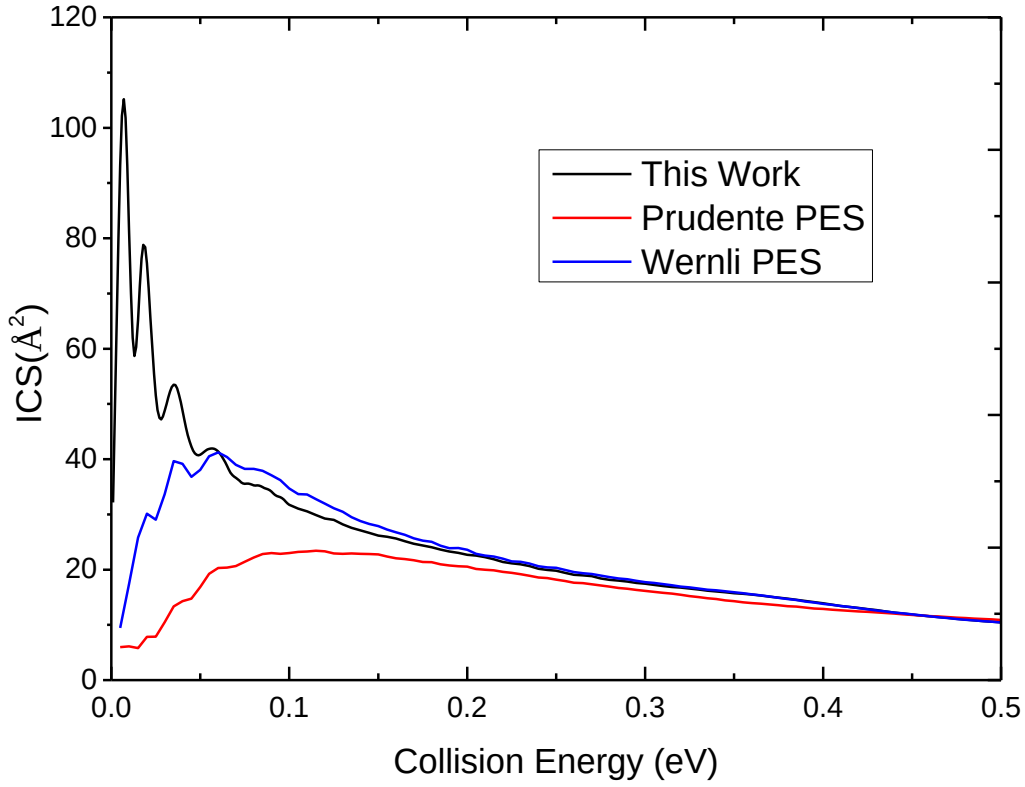

Fig. 6 Total ICSs of the H(^{2}S) + LiH($X^1\Sigma^+$) → Li(^{2}S) + H_2($X^1\Sigma_g^+$) reaction calculated by TDWP method on the present PES, Prudente PES [Ref. 18] and Wernli PES [Ref. 17].

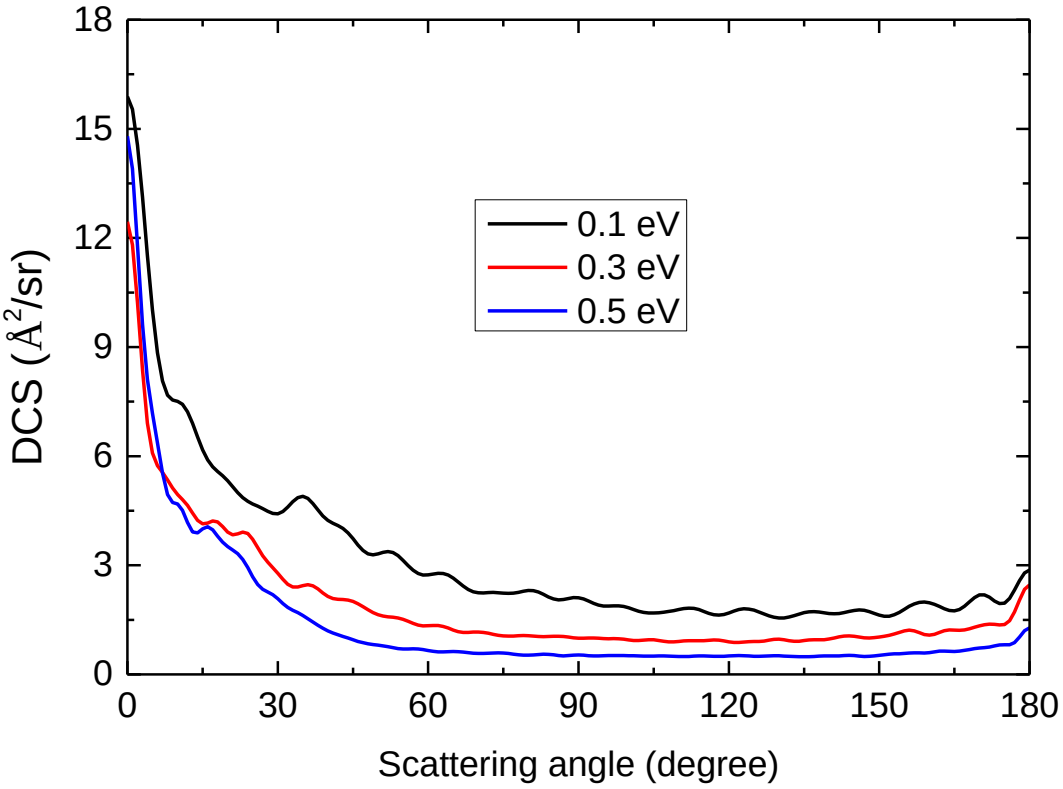

Fig. 7 DCSs of the $H(^2S) + LiH(X^1\Sigma^+) \rightarrow Li(^2S) + H_2(X^1\Sigma_g^+)$ reaction at three collision energies (0.1 eV, 0.3 eV and 0.5 eV).